Anisotropy of the pairing gap of FeAs-based superconductors induced by spin fluctuations

Rastko Sknepnek, German Samolyuk,[*] Yong-bin Lee, and Jörg Schmalian
Department of Physics and Astronomy and Ames Laboratory, Iowa State University, Ames, Iowa 50011, USA
(Received 24 December 2008; published 11 February 2009)

We determine the anisotropy of the spin-fluctuation-induced pairing gap on the Fermi surface of the FeAs-based superconductors as function of the exchange and Hund's coupling J_H. We find that for sufficiently large J_H, nearly commensurate magnetic fluctuations yield a fully gapped $s^{\pm}$-pairing state with small anisotropy of the gap amplitude on each Fermi-surface sheet, but significant variations of the gap amplitude for different sheets of the Fermi surface. In particular, we obtain the large variation of the gap amplitude on different Fermi-surface sheets, as seen in angular resolved photoemission spectroscopy experiments. For smaller values of Hund's coupling incommensurate magnetic fluctuations yield an $s^{\pm}$-pairing state with line nodes. Such a state is also possible once the anisotropy of the material is reduced and three-dimensional effects come into play.

I. INTRODUCTION

The recently discovered FeAs-based family[1] has been captivating the community primarily because of its high superconducting transition temperatures, with T_c values well above 50 K in some cases.[2–5] While such values for T_c could potentially be due to the interaction between electrons and lattice vibrations, the vibrational modes of the common structural unit, the FeAs planes, are rather low, making electron-phonon interactions as the sole or primary mechanism unlikely.[6] The observation of antiferromagnetic order in undoped systems at ambient pressure[7] has therefore been one of the key motivations to explore spin fluctuations as the primary mechanism for superconductivity in the pnictides.[8–10] In this case, the role of phonons, as intermediate boson and pairing glue, is being played by collective paramagnon excitations of the electron fluid. In order to determine which many-body interaction is responsible for the formation of Cooper pairs, an understanding of the symmetry and detailed momentum dependence of the pairing gap is crucial.

Experimentally, the strongest indication that the pairing gap in the pnictides has line nodes comes from nuclear magnetic resonance (NMR) measurement with power-law variation of the spin-lattice relaxation rate, $T_1^{-1} \propto T^3$.[11–14] On the other hand angular resolved photoemission spectroscopy (ARPES) experiments find nodeless weakly anisotropic gaps on the Fermi surface.[15–17] Penetration depth measurements in the 122-compound $Ba_{0.93}Co_{0.07}Fe_2As_2$ support gap nodes,[18] while measurements for the 1111 system $NdFeAsO_{0.9}F_{0.1}$ favor anisotropic gaps that remain finite everywhere on the Fermi surface.[19] Interestingly, NMR results of Ref. 12 and the ARPES data of Refs. 16 and 17 are consistent to the extent that they see evidence for multiple gap values. ARPES measurements demonstrate that the two Fermi-surface sheets around the Γ point of $Ba_{0.6}K_{0.4}Fe_2As_2$ have amplitudes that differ by more than a factor of 2.[17] Knight shift and spin-lattice relaxation rate measurements in $PrFeAsO_{0.89}F_{0.11}$ were fit to two gaps with ratio $\simeq 3.2$.[12]

In this paper we determine the momentum dependence of the superconducting gap, where Cooper pairing is due to the exchange of antiferromagnetic spin fluctuations. We find, in agreement with previous calculations,[8,9,20,21] that the pairing symmetry is extended s wave with the gap on different Fermi-surface sheets being out of phase, i.e., we find an $s^{\pm}$ pairing state. Superconductivity is caused by the enhanced collective spin fluctuations in the proximity to an ordered antiferromagnetic state. We find that commensurate magnetic correlations can be caused by including a sufficiently large Hund's rule coupling J_H, even in an itinerant magnetic material. We also find that a large Hund's coupling generally yields a stronger tendency toward superconductivity where transition temperatures of 50 K are possible. We demonstrate that the gap function is weakly anisotropic for most sheets of the Fermi surface, while a significant anisotropy remains. Depending on the strength of the exchange and Hund's couplings J_H the gap of this Fermi-surface sheet vanishes on line nodes (for small J_H) or exhibits a moderately anisotropic variation along the Fermi surface (for larger, more realistic values of J_H). We also comment on the fact that a sizable interlayer coupling, as relevant for the 122 FeAs family, might lead to a nodal superconducting state, while for the more anisotropic 1111 family a fully gapped state is more likely. A possible explanation for the conflicting ARPES and NMR findings is that experiments sensitive to the maximum of the gap, such as ARPES, see large gaps, while experiments sensitive to the minimum of the gap, such as NMR, find nodelike features due to impurity-induced states in the gap.[21] The latter is due to the fact that nonmagnetic impurities in an $s^{\pm}$ pairing state behave like pair breaking magnetic impurities in a conventional s-wave superconductor.

The spin-fluctuation approach relies on two key assumptions:[22] (i) the proximity to a magnetic instability with paramagnons as relevant collective modes and (ii) conventional Fermi-liquid behavior away from the instability. While electronic correlations of the Fe $3d$ orbitals in the pnictides are relevant, the multiorbital nature of the system is likely the reason that strong local correlations reminiscent of a system close to a Mott insulating state do not seem to be dominating. In addition, the carrier density of the FeAs systems does not seem to be anywhere close to an odd number of electrons per Fe $3d$ site, strongly suggesting that there are no Mott-Hubbard bands with appreciable spectral weight.

Rather, these systems are closer in their behavior to band insulators or semimetals, however with the bottom of the electron band somewhat below the top of a hole band. The latter leads to the observed hole and electron sheets of the Fermi surface. Consistent with this picture is that undoped ambient pressure systems exhibit a small but well-established Drude conductivity[23] and magneto-oscillations[24] in what seems to be a partially gapped metallic antiferromagnetic state. Above the magnetic ordering temperature a sizable Drude weight not untypical for an almost semimetal has been observed. The magnetic susceptibility of $BaFe_2As_2$ single crystals[25] above the magnetic transition is only very weakly temperature dependent and shows no sign for local-moment behavior of the Fe $3d$ electron spins. X-ray absorption spectroscopy for $LaFeAsO_{1-x}F_x$ is consistent with a rigid-band filling on F doping and moderate values for the effective Hubbard interaction.[26] Clearly, these observations do not imply that the interactions in the FeAs systems are weak, but rather that the phase space for strong local correlations is limited and suggest that predominant electron-electron interactions are related to interband scattering between the hole and electron sheets of the Fermi surface. Despite very interesting approaches based on the assumption that the FeAs system are doped Mott insulators,[27,28] we take the view that the iron pnictides may be good examples for a system where collective longer-ranged spin and charge excitations play an important role.

As shown first by Berk and Schrieffer,[29] magnetic fluctuations suppress pairing for a gap function $\Delta_{a_1a_2}(\mathbf{p}) = \Delta_0$ that is constant as function of momentum $\mathbf{p}$ and band indices a_i. However, changing the sign of $\Delta_{a_1a_2}(\mathbf{p})$ as function of either $\mathbf{p}$ or a_1, a_2 allows for nontrivial superconducting states due to paramagnon fluctuations and makes such fluctuations a powerful pairing mechanism. In case where only one band contributes to the Fermi surface the sign change is a function of momentum $\mathbf{p}$ and may lead to line or point nodes of the gap. If there are several bands crossing the Fermi energy, strong interband scattering can lead to a sign change of the gap between different Fermi-surface sheets without leading to gap nodes. The $s^{\pm}$-pairing state that results from our analysis was proposed in the context of the FeAs systems in Ref. 8 in a model with structureless (in momentum state) interband pairing interactions. In such a state, one would always obtain fully gapped Fermi-surface sheets. Our analysis shows that the model of Ref. 8 captures the $s^{\pm}$ state properly but that one needs to include the momentum dependence of the pairing interaction to obtain states with residual anisotropy of the pairing gap, including states that possess nodes of the gap on a given Fermi-surface sheet. A careful investigation of the role of interband scattering in systems with close to perfect nesting between distinct Fermi-surface sheets was performed in Refs. 20 and 21. These approaches demonstrate that under certain circumstances, pairing interactions are enhanced due to interband nesting. At the level of the weak-coupling expansion used in Ref. 21, this conclusion does depend on whether the pairing mechanism is due to spin-orbital or charge fluctuations. Our results are consistent with these findings, but favor a spin-fluctuation mechanism boosted by intrasite and interorbital exchanges and Hund's rule coupling. Our approach is closest to the results of Refs. 9 and

30. The key emphasis in our work, as compared to these interesting investigations, is to quantitatively analyze the variation of the pairing gap on individual Fermi-surface sheets as well as between distinct sheets.

II. MODEL

Electronic structure calculations clearly show that the states close to the Fermi level are predominantly of Fe $3d$ character with several sheets of the Fermi surface,[31] as confirmed in recent ARPES experiments.[15–17,32] Given the need to change the sign of the gap function $\Delta_{a_1a_2}(\mathbf{p})$, this leads to the proposal by Mazin *et al.*[8] that the gap function on sheets coupled by the magnetic wave vector are out of phase.

We use a tight-binding description of the Fe d_{xz}, d_{yz} states of the FeAs systems identical to the one proposed by Raghu *et al.*[33] There are two Fe atoms per crystallographic unit cell leading to the tight-binding Hamiltonian

$$H_0 = \sum_{\mathbf{p},\alpha\beta,\sigma} E_{\mathbf{p}}^{\alpha\beta} d_{\mathbf{p}\alpha\sigma}^{\dagger} d_{\mathbf{p}\beta\sigma}, \tag{1}$$

where $d_{\mathbf{p}\alpha\sigma}^{\dagger}$ is the creation operator of an electron with momentum $\mathbf{p}$ and spin σ. α refers to the orbital degree (i.e., xz and yz) as well as the label of the Fe atom within the unit cell. Momenta go from $-\pi/a$ to π/a, where $a = \sqrt{2}a_0$ with Fe-Fe distance a_0. Thus $\hat{E}_{\mathbf{p}}$ is a (4×4) matrix. As in Ref. 33 we assume, for simplicity, that all As atoms in the unit cell are identical. This approximation seems justified as there are virtually no As states close to the Fermi level. The primary relevance of the As states is only to determine the indirect overlap between Fe orbitals on different sites. With these assumptions, we obtain a block structure for the tight-binding Hamiltonian of the form

$$\hat{E}_{\mathbf{p}} = \hat{h}_{\mathbf{p}} \otimes \hat{1} + \hat{\delta}_{\mathbf{p}} \otimes \hat{\tau}_x, \tag{2}$$

with (2×2) unit matrix $\hat{1}$ and Pauli matrix $\hat{\tau}_x$. $\hat{h}_{\mathbf{p}}$ is a diagonal (2×2) matrix with diagonal elements

$$h_{\mathbf{p}}^{11} = 2t_2 \cos(p_x a) + 2t_3 \cos(p_y a),$$

$$h_{\mathbf{p}}^{22} = 2t_3 \cos(p_x a) + 2t_2 \cos(p_y a). \tag{3}$$

Both diagonal elements of the (2×2) matrix $\hat{\delta}_{\mathbf{p}}$ are

$$\delta_{\mathbf{p}}^{11} = \delta_{\mathbf{p}}^{22} = 4t_5 \cos\left(\frac{p_x a}{2}\right) \cos\left(\frac{p_y a}{2}\right), \tag{4}$$

while the off-diagonal elements are

$$\delta_{\mathbf{p}}^{12} = \delta_{\mathbf{p}}^{21} = 4t_6 \sin\left(\frac{p_x a}{2}\right) \sin\left(\frac{p_y a}{2}\right). \tag{5}$$

The individual parameters, determined from fits to full potential density-functional calculations for LaFeAsO, are $t_2 = 0.495$, $t_3 = -0.026$, $t_5 = -0.026$, and $t_6 = -0.36$ eV.

Because of the assumption of treating all As atoms identically, regardless of whether they are located above or below the Fe planes, we can describe the system in a unit cell with only one Fe atom and can upfold the band structure into a
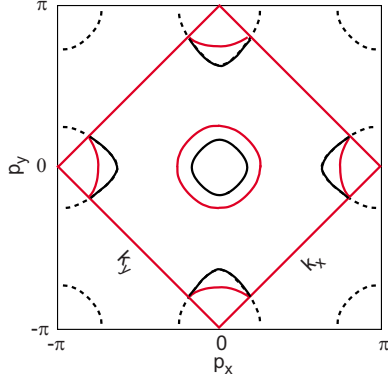
FIG. 1. (Color online) Fermi surface of the tight-binding parametrization described in the text in the Brillouin zone that corresponds to two Fe atoms per unit cell (red diamond with axes labeled by k_x and k_y) and the larger Brillouin zone that corresponds to a unit cell with one atom per unit cell (solid square with axes labeled by p_x and p_y), respectively.

larger Brillouin zone, i.e., we obtain a (2×2) matrix tight binding $\hat{\varepsilon}_\mathbf{k}$ in the larger Brillouin zone. It holds $\hat{h}_\mathbf{p} = \hat{h}_{\mathbf{p}+\mathbf{G}}$ and $\hat{\delta}_{\mathbf{p}+\mathbf{G}} = -\hat{\delta}_\mathbf{p}$ with reciprocal-lattice vector $\mathbf{G} = (\frac{2\pi}{a}, 0)$ and we obtain a $\hat{\varepsilon}_\mathbf{k} = \hat{h}_\mathbf{p} + \hat{\delta}_\mathbf{p}$ for states in the original smaller Brillouin zone and $\hat{\varepsilon}_{\mathbf{k}+\mathbf{G}} = \hat{h}_\mathbf{p} - \hat{\delta}_\mathbf{p}$ for momenta outside of it. The momentum $\mathbf{k}$ in the new larger Brillouin zone, with $-\frac{\pi}{a_0} \le k_{x,y} < \frac{\pi}{a_0}$, is given by $k_x = \frac{1}{\sqrt{2}}(p_x - p_y)$ and $k_y = \frac{1}{\sqrt{2}}(p_x + p_y)$. For example, the wave vector of the spin-density wave $\mathbf{Q} = (\frac{\pi}{a}, \frac{\pi}{a})$ becomes $\mathbf{Q} = (0, \frac{\pi}{a_0})$ in the larger BZ.

In Fig. 1 we show the Fermi surface that results from the above tight-binding parametrization at a density $n = 1.05$. To illustrate the two Brillouin zones used in the above discussion we plot the Fermi surface in an extended zone scheme. To make contact with Ref. 33, we note that the axes defining the d_{xz} and d_{yz} orbitals are rotated by $\pi/4$ relative to each other.

Next we include the local electron-electron interaction into our theory and write

$$H_{\text{int}} = U \sum_{i,a} n_{ia\uparrow} n_{ia\downarrow} + U' \sum_{i,a>b} n_{ia} n_{ib} - J_H \sum_{i,a>b} \left(2\mathbf{s}_{ia} \cdot \mathbf{s}_{ib} \right.$$
$$\left. + \frac{1}{2} n_{ia} n_{ib} \right) + J \sum_{i,a>b,\sigma} d^\dagger_{ia\sigma} d^\dagger_{ia\bar{\sigma}} d_{ib\bar{\sigma}} d_{ib\sigma}, \quad (6)$$

where $n_{ia\sigma} = d^\dagger_{ia\sigma} d_{ia\sigma}$ is the occupation of the orbital a with spin σ at site i. $n_{ia} = \sum_\sigma n_{ia\sigma}$ is the total charge in this orbital and $\mathbf{s}_{ia} = \frac{1}{2} \sum_{\sigma\sigma'} d^\dagger_{ia\sigma} \boldsymbol{\sigma}_{\sigma\sigma'} d_{ia\sigma'}$ the corresponding spin. Thus, we include intra- and interorbital direct Coulomb interactions, U and U', as well as the Hund's rule coupling J_H and the exchange interaction J. The latter are of interest as they affect the spin correlations of electrons in different orbitals. In what follows we use $U=1$ eV, $U'=0.5$ eV, electron density $n=1.05$ per site and spin (as follows from fit to our full potential density functional calculation for LaFeAsO), and we vary $J=J_H$ between $J=0$ and $J=0.5$ eV to explore the role of the exchange and Hund's interactions on the pairing

state. Recent x-ray absorption spectroscopy measurements support values for the Hund's couplings that lead to a preferred high spin configuration,[26] leading to larger values of $J_H \lesssim U$.

The interaction term can be put into a more compact form[34]

$$H_{\text{int}} = \frac{1}{4} \sum_{i,a_l;\sigma_l} U^{a_1 a_2, a_3 a_4}_{\sigma_1 \sigma_2, \sigma_3 \sigma_4} d^\dagger_{ia_1\sigma_1} d^\dagger_{ia_2\sigma_2} d_{ia_3\sigma_3} d_{ia_4\sigma_4}, \quad (7)$$

and, in the absence of spin orbit interaction, split into a spin and a charge contribution

$$U^{a_1 a_2, a_3 a_4}_{\sigma_1 \sigma_2, \sigma_3 \sigma_4} = -\frac{1}{2} U^{a_1 a_4, a_2 a_3}_s \boldsymbol{\sigma}_{\sigma_1\sigma_4} \cdot \boldsymbol{\sigma}_{\sigma_2\sigma_3} + \frac{1}{2} U^{a_1 a_4, a_2 a_3}_c \delta_{\sigma_1\sigma_4} \delta_{\sigma_2\sigma_3}. \quad (8)$$

The above Hamiltonian is then recovered if we chose

$$U^{a_1 a_4, a_2 a_3}_s = \begin{cases} U & \text{if } a_1 = a_2 = a_3 = a_4 \\ U' & \text{if } a_1 = a_3 \ne a_2 = a_4 \\ J_H & \text{if } a_1 = a_4 \ne a_2 = a_3 \\ J & \text{if } a_1 = a_2 \ne a_3 = a_4 \end{cases} \quad (9)$$

for the spin part of the interaction and

$$U^{a_1 a_4, a_2 a_3}_c = \begin{cases} U & \text{if } a_1 = a_2 = a_3 = a_4 \\ -U' + 2J_H & \text{if } a_1 = a_3 \ne a_2 = a_4 \\ 2U' - J_H & \text{if } a_1 = a_4 \ne a_2 = a_3 \\ J & \text{if } a_1 = a_2 \ne a_3 = a_4 \end{cases} \quad (10)$$

for the corresponding charge contribution, respectively.

A. Collective spin and charge fluctuations

We determine the single particle and collective magnetic excitation spectrum within a self-consistent one-loop approach, the multiple orbital version[34,35] of the fluctuation exchange approximation of Ref. 36. Once we have self-consistently determined the fermionic Green's function $G^{ab}(k)$, where $k = (\mathbf{k}, \omega_n)$ stands jointly for the crystal momentum $\mathbf{k}$ and the Matsubara frequency $\omega_n = (2n+1)\pi T$, we determine the symmetry of the pairing state from the linearized gap equation. In the normal state, the matrix Green's function of the problem is

$$\hat{G}(k) = [i\omega_n \hat{1} - \hat{\varepsilon}_\mathbf{k} - \hat{\Sigma}(k)]^{-1}, \quad (11)$$

where $\hat{G}_k$, $\hat{\Sigma}_k$, and $\hat{\varepsilon}_\mathbf{k}$ are all 2×2 matrices in orbital space in the larger Brillouin zone. The self-energy is given as a sum of a Hartree-Fock contribution and a fluctuation term

$$\Sigma^{a_1 a_2}(k) = \sum_{k'} \sum_{a_3 a_4} G^{a_3 a_4}(k') \Gamma^{a_1 a_3, a_4 a_2}_{\text{ph}}(k - k'), \quad (12)$$

where $\Sigma_k \ldots = \frac{T}{N^2} \sum_{\mathbf{k},n} \ldots$ includes the summation over momenta and over Matsubara frequencies.

Introducing the particle quantum numbers $A = (a_1, a_2)$ and $B = (a_3, a_4)$ labeling the rows and columns of two-particle states interaction, $\Gamma^{a_1 a_3, a_4 a_2}_{\text{ph}}(q) = \Gamma^{AB}_{\text{ph}}(q)$ becomes a 4×4-dimensional symmetric operator $\tilde{\Gamma}_{\text{ph}}(q)$. Similarly we

obtain in this two-particle basis a matrix representation for the spin and charge couplings $\widetilde{U}^s$ and $\widetilde{U}^c$,

$$\widetilde{U}^s = \begin{pmatrix} U & 0 & 0 & J_H \\ 0 & U' & J & 0 \\ 0 & J & U' & 0 \\ J_H & 0 & 0 & U \end{pmatrix} \quad (13)$$

and

$$\widetilde{U}^c = \begin{pmatrix} U & 0 & 0 & W \\ 0 & W' & J' & 0 \\ 0 & J' & W' & 0 \\ W & 0 & 0 & U \end{pmatrix}, \quad (14)$$

where $W = 2U' - J_H$ and $W' = 2J_H - U'$. In this two-particle formalism it is now straightforward to sum particle-hole ladder and bubble diagrams and it follows

$$\widetilde{\Gamma}_{ph}(q) = \frac{3}{2}\widetilde{V}^s(q) + \frac{1}{2}\widetilde{V}^s(q), \quad (15)$$

with

$$\widetilde{V}^s(q) = \widetilde{U}^s[1 - \widetilde{\chi}(q)\widetilde{U}^s]^{-1}\widetilde{\chi}(q)\widetilde{U}^s - \frac{1}{2}\widetilde{U}^s\widetilde{\chi}(q)\widetilde{U}^s, \quad (16)$$

$$\widetilde{V}^c(q) = \widetilde{U}^c[1 + \widetilde{\chi}(q)\widetilde{U}^c]^{-1}\widetilde{\chi}(q)\widetilde{U}^c - \frac{1}{2}\widetilde{U}^c\widetilde{\chi}(q)\widetilde{U}^c. \quad (17)$$

Here $\widetilde{\chi}(q)$ is the matrix of particle-hole bubble in the two-particle basis. Explicitly it holds

$$\chi^{a_1 a_2, a_3 a_4}(q) = -\frac{T}{N^2}\sum_k G^{a_2 a_3}(k+q)G^{a_4 a_1}(q). \quad (18)$$

The Hartree-Fock term of the self-energy

$$\Sigma_{HF}^{a_1 a_2} = \sum_{a_3 a_4}\left(\frac{3}{2}\widetilde{U}^{s,a_3 a_1, a_4 a_2} - \frac{1}{2}\widetilde{U}^{c,a_3 a_1, a_4 a_2}\right)G_0^{a_3 a_4}(\tau^-) \quad (19)$$

is frequency and momentum independent and determined by $G_0^{a_3 a_4}(\tau^-) = \langle d_{0a_3}^\dagger d_{0a_4}\rangle$. It holds for the diagonal elements

$$\Sigma_{HF}^{a_1 a_1} = Un_{a_1} + (2U' - J_H)\sum_{a_2 \neq a_1} n_{a_2}$$

$$= (U - 2U' + J_H)n_{a_1} + (2U' - J_H)n, \quad (20)$$

whereas the off-diagonal elements $(a_1 \neq a_2)$ are given as

$$\Sigma_{HF}^{a_1 a_2} = (2J_H + J - U')\langle d_{0,a_1}^\dagger d_{0,a_2}\rangle. \quad (21)$$

We are interested in the superconducting transition temperature and the symmetry of the superconducting state, determined by the corresponding anomalous self-energy $\hat{\Phi}_{\mathbf{k}}(\omega_n)$. Summing up the same class of diagrams in the superconducting state yields

$$\Phi^{a_1 a_2}(k) = \sum_{k' a_3 a_4} \Gamma_{pp}^{a_3 a_1, a_2 a_4}(k - k')F^{a_3 a_4}(k'), \quad (22)$$

with Gor'kov function $\hat{F}(k)$. $\widetilde{\Gamma}_{pp}(q)$ is the corresponding operator in the two-particle representation. In this paper we only solve the linearized version of Eq. (22) to determine the superconducting transition temperature as well as the nature of the pairing state right below T_c. Close to the superconducting transition temperature we linearize the anomalous propagator

$$\hat{F}(k) \simeq -\hat{G}(k)\hat{\Phi}(k)\hat{G}(-k) \quad (23)$$

and obtain

$$\Phi^{a_1 a_2}(k) = -\frac{T}{N^2}\sum_{k' a_3 a_4 a_5 a_6} \Gamma_{pp}^{a_3 a_1, a_2 a_4}(k - k')G^{a_3 a_5}(k')$$

$$\times \Phi^{a_5 a_6}(k')G^{a_6 a_4}(-k'). \quad (24)$$

Since $F^{a_3 a_4}(k')$ is of first order in the anomalous self-energy $\Phi^{a_1 a_2}(k)$, the linearized version of Eq. (24) is determined by $\widetilde{\Gamma}_{pp}(q)$ for $\Phi^{a_1 a_2}(k) = 0$. In this limit it follows, after summing the same bubble and ladder diagrams as for $\widetilde{\Gamma}_{ph}(q)$ that

$$\widetilde{\Gamma}_{pp}(q) = \frac{3}{2}\widetilde{V}^s(q) - \frac{1}{2}\widetilde{V}^c(q), \quad (25)$$

with

$$\widetilde{V}^s(q) = \widetilde{U}^s[1 - \widetilde{\chi}(q)\widetilde{U}^s]^{-1}\widetilde{\chi}(q)\widetilde{U}^s + \frac{\widetilde{U}^s}{2},$$

$$\widetilde{V}^c(q) = \widetilde{U}^c[1 + \widetilde{\chi}(q)\widetilde{U}^c]^{-1}\widetilde{\chi}(q)\widetilde{U}^c - \frac{\widetilde{U}^c}{2}. \quad (26)$$

In what follows we first solve the coupled equations Eqs. (12), (15), (16), and (18) in the normal state on a 32×32 lattice with 2^{11} Matsubara frequencies. The solutions of the normal-state equations are then used to solve the linearized equation for the superconducting self-energy. In order to determine the superconducting transition temperature we replace $\Phi^{a_1 a_2}(p)$ on the left-hand side of Eq. (24) by $\lambda\Phi^{a_1 a_2}(p)$. The resulting eigenvalue equation yields an eigenvalue $\lambda = 1$ if $T = T_c$, i.e., the temperature where the linearization is permitted. For $T > T_c$, it holds $\lambda < 1$ for the largest eigenvalue. Even if $\lambda < 1$, the result is still useful as $(1 - \lambda)^{-1}$ is proportional to the pairing correlation function. Most importantly, the eigenvector of the leading eigenvalue determines the momentum and band-index dependence of the gap right below T_c. In order to simplify the above eigenvalue equation we replace $\widetilde{\Gamma}_{pp}(p)$ by its zero Matsubara frequency value, i.e., $\widetilde{\Gamma}_{pp}(\mathbf{p}, \omega_n = 0)$. Thus, we keep the dynamic excitations that determine the frequency dependence of the normal-state single-particle self-energy, but assume that the dynamics of the pairing interaction is structureless. Such an approximation would be problematic close to a magnetic quantum critical point with diverging antiferromagnetic correlation length,[37] but is expected to be reasonable for intermediate magnetic correlations, as seems to be the case in the FeAs

systems. A consequence of this approximation is that we lose the information about the frequency dependence of the anomalous self-energy. We keep its momentum and orbital index dependence.

B. Symmetry considerations

For a proper interpretation of the momentum dependence of the superconducting gap in a multiorbital problem, we analyze the point-group symmetry of the two-band model describing the d_{xz} and d_{yz} orbitals. We consider the behavior of the Hamiltonian under the tetragonal point group $D_{4h} = C_{4v} \otimes C_i$, where C_i is the inversion and C_{4v} contains next to the identity E two fourfold rotations c_4, one twofold rotation c_2, two mirror reflexions along the axis σ_v, and two mirror reflexions along the diagonals σ_d. The Hamiltonian is invariant with respect to the group D_{4h}, i.e.,

$$\hat{\varepsilon}_{\mathbf{k}} = R\hat{\varepsilon}_{\mathbf{k}} \quad \text{for all} \quad R \in D_{4h}. \tag{27}$$

Since the two orbitals d_{xz} and d_{yz} transform like coordinates for in-plane symmetry operations, it holds

$$R\hat{\varepsilon}_{\mathbf{k}} = D_R^{(1)}\hat{\varepsilon}_{D_R^{(1)}\mathbf{k}}(D_R^{(1)})^{-1}, \tag{28}$$

where $D_R^{(1)}$ is the representation of R which transforms the coordinates. It then follows that the spinor

$$c_{\mathbf{k}\sigma} = \begin{pmatrix} c_{\mathbf{k},xz,\sigma} \\ c_{\mathbf{k},yz,\sigma} \end{pmatrix} \tag{29}$$

transforms as

$$Rc_{\mathbf{k}} = D_R^{(1)-1}c_{D_R^{(1)}\mathbf{k}}, \tag{30}$$

which determines the transformation properties of the superconducting gap function in the singlet channel

$$R\Phi_{\mathbf{k}}^{ab} = \sum_{a'b'} D_{Raa'}^{(1)-1}D_{Rbb'}^{(1)-1}\Phi_{D_R^{(1)}\mathbf{k}}^{a'b'}. \tag{31}$$

It follows for the transformation of the gap under the point-group operations

$$E\hat{\Phi}_{(k_x,k_y)} = \begin{pmatrix} \Phi_{(k_x,k_y)}^{xx} & \Phi_{(k_x,k_y)}^{xy} \\ \Phi_{(k_x,k_y)}^{yx} & \Phi_{(k_x,k_y)}^{yy} \end{pmatrix},$$

$$C_4\hat{\Phi}_{(k_x,k_y)} = \begin{pmatrix} \Phi_{(k_y,-k_x)}^{yy} & -\Phi_{(k_y,-k_x)}^{yx} \\ -\Phi_{(k_y,-k_x)}^{xy} & \Phi_{(k_y,-k_x)}^{xx} \end{pmatrix},$$

$$C_2\hat{\Phi}_{(k_x,k_y)} = \begin{pmatrix} \Phi_{(-k_x,-k_y)}^{xx} & \Phi_{(-k_x,-k_y)}^{xy} \\ \Phi_{(-k_x,-k_y)}^{yx} & \Phi_{(-k_x,-k_y)}^{yy} \end{pmatrix},$$

$$\sigma_v\hat{\Phi}_{(k_x,k_y)} = \begin{pmatrix} \Phi_{(k_x,-k_y)}^{xx} & -\Phi_{(k_x,-k_y)}^{xy} \\ -\Phi_{(k_x,-k_y)}^{yy} & \Phi_{(k_x,-k_y)}^{yy} \end{pmatrix},$$
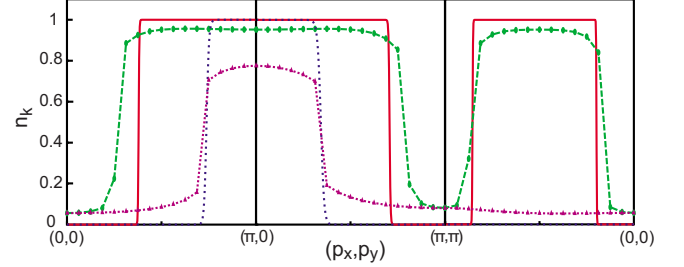

FIG. 2. (Color online) Band occupation number along $(0,0) \to (\pi,0) \to (\pi,\pi) \to (0,0)$ for noninteracting case (red and blue) and with interactions (green and violet).

$$\sigma_d\hat{\Phi}_{(k_x,k_y)} = \begin{pmatrix} \Phi_{(k_y,k_x)}^{yy} & \Phi_{(k_y,k_x)}^{yx} \\ \Phi_{(k_y,k_x)}^{xy} & \Phi_{(k_y,k_x)}^{xx} \end{pmatrix}. \tag{32}$$

A rotation by $\pi/2$ that causes a sign change of an off-diagonal element of $\hat{\Phi}$ is therefore not an indication for pairing in the d-wave channel. Thus assuming a rotation by $\pi/2$ (as generated by C_4) yields a sign change of the off-diagonal element and no such change occurs for the diagonal element; we find $C_4\hat{\Phi}_{(k_x,k_y)} = \hat{\Phi}_{(k_x,k_y)}$, i.e., the gap belongs either to the irreducible representation A_1 or A_2. If furthermore the gap does not change sign upon reflection on the axis we conclude it is A_1, corresponding to s-wave pairing. This will be the case in our subsequent analysis of the numerical solution of spin-fluctuation-induced pairing.

III. RESULTS

In Fig. 2 we show the occupation number $n_{\mathbf{p}}$ determined from the full solution of the self-consistent equations in the normal state at $T = 0.004$ eV. We compare our results to the corresponding occupation of the tight-binding model without interaction at the same filling. The electron band closest to $\mathbf{p} = (\pi/a, 0)$ undergoes a substantial distribution of carriers as it is being pushed very close to the Fermi energy. Similarly we observe a decrease in the Fermi-surface volume of the hole band centered around $\mathbf{p} = (0,0)$. Still the overall shape and topology of the various Fermi-surface sheets are unchanged by many-body interactions.

In Fig. 3 we show the momentum dependence of the $a_i = 0$ component of the effective interaction $\Gamma_{\text{ph}}^{a_1 a_3, a_4 a_2}(\mathbf{p}, \omega_n = 0)$. This is one of the dominating components. Other matrix elements of $\tilde{\Gamma}_{\text{ph}}(q)$ have a similar momentum dependence. Finally $\tilde{\Gamma}_{\text{ph}}(q)$ and the particle-particle interaction $\tilde{\Gamma}_{\text{pp}}(q)$ behave very similar. The three panels show the effective interaction mediated by collective spin and charge fluctuations for three different values of the Hund's coupling J_H. We clearly see that the effect of J_H is twofold. On the one hand, larger values of the exchange coupling lead to an increase of the Stoner enhancement in Γ_{pp} and Γ_{ph}. In addition, the effective interaction becomes increasingly more commensurate as J_H increases. The strong peaks close to $\mathbf{p} = (\pm\pi/a, 0)$ and $\mathbf{p} = (0, \pm\pi/a)$ are consistent with the observed Bragg peaks for the magnetic ordering in the undoped parent compounds.[7]
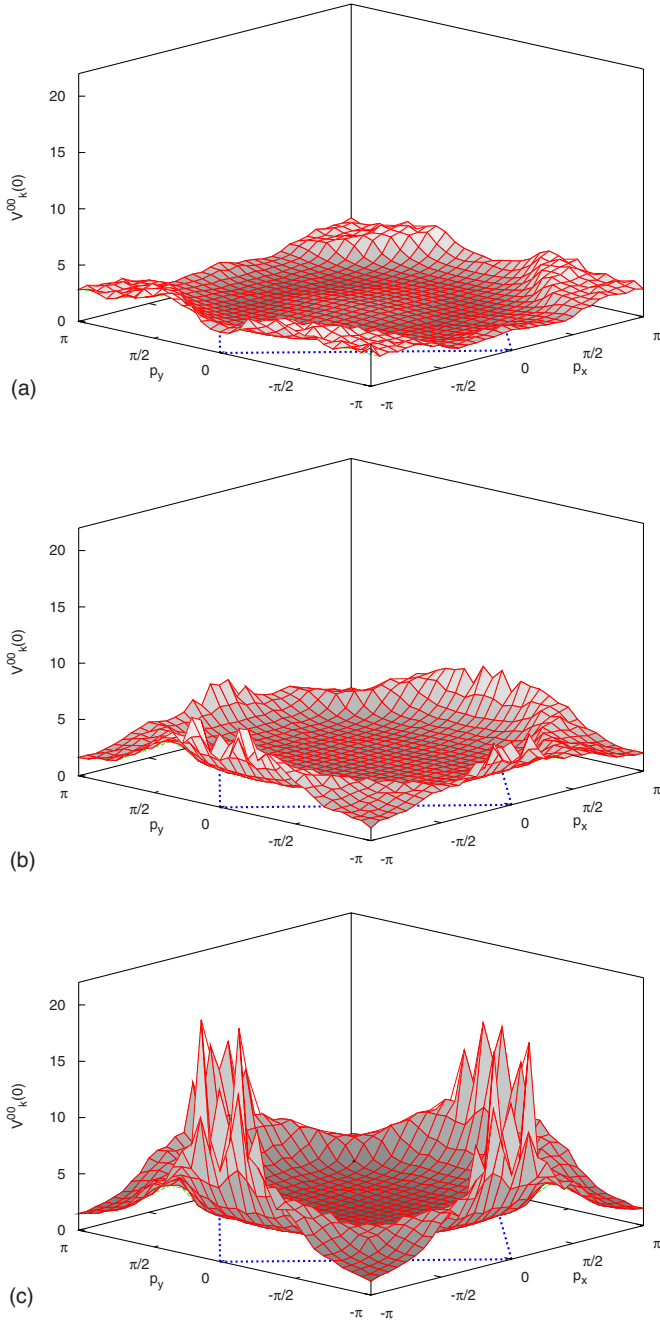
(a)

(b)

(c)

FIG. 3. (Color online) $a_3a_1, a_2a_4 = (0,0)$ component of the pairing interaction $\Gamma_{ph}^{a_3a_1,a_2a_4}(\mathbf{p}, \omega_n = 0)$, Eq. (15), for (a) $J = 0.0$, (b) 0.25, and (c) 0.50 eV. Pairing interaction becomes increasingly commensurate as the Hund's coupling J increases.

In Fig. 4 we show the variation of the largest eigenvalue λ as function of the exchange and Hund's coupling J for two temperatures $T = 0.004$ eV $\simeq 46$ K and $T = 0.006$ eV $\simeq 70$ K. The enhancement of the effective pairing interaction, discussed in Fig. 3, is the primary reason for the enhancement of the pairing strength and, in turn, of the leading eigenvalue λ. We also find that $\lambda = 1$ for $J \simeq 0.4$ eV, which would correspond to a critical temperature $T_c \simeq 70$ K. While the above-mentioned static approximation tends to overestimate T_c, these results demonstrate that experimentally rel-
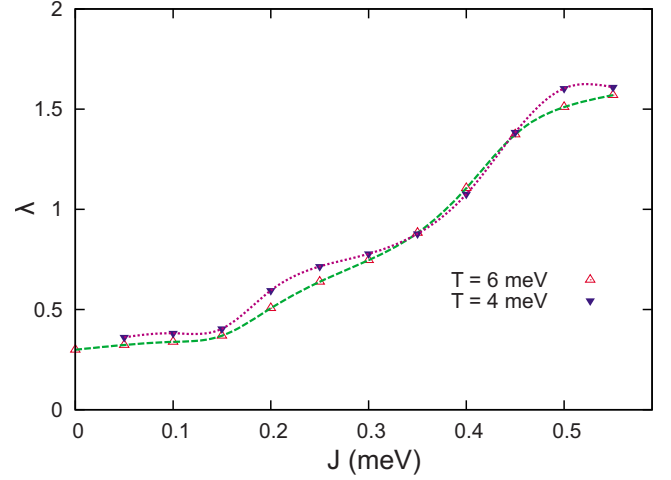

FIG. 4. (Color online) Largest eigenvalue λ for the linearized version of Eq. (24) with $\Gamma^{a_3a_1,a_2a_4}(\mathbf{p}, \omega_n = 0)$ as a function of Hund's coupling J for $T = 0.004$ and 0.006 eV.

evant T_c values are clearly possible within the spin-fluctuation approach.

In Fig. 5 we show the momentum dependence of $\Delta_{xx}(\mathbf{p})$ and $\Delta_{xy}(\mathbf{p})$ as determined from the leading eigenvector of the linearized gap equation at $T = 0.006$ eV. The indicated diamond corresponds to the Brillouin-zone boundary, i.e., we plot the gap of the two xz orbitals within the unit cell in an extended zone scheme. The fact that both gap functions are of comparable magnitude reflects the fact that Cooper pairs are formed out of electrons in the same and in different d states. The symmetry of the gap function is s wave, i.e., it is invariant with respect to the point-group operations of the Hamiltonian. Simultaneous rotation of momenta $\mathbf{p}$ and orbitals by $\pi/2$ yields $\Delta_{xx}(p_x, p_y) \rightarrow \Delta_{yy}(p_y, -p_x)$ and $\Delta_{xy}(p_x, p_y)$
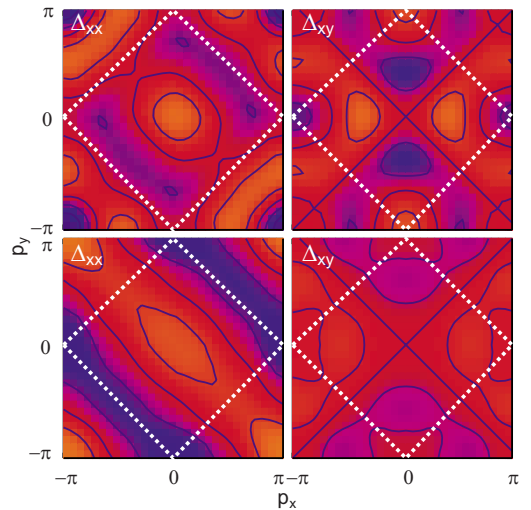

FIG. 5. (Color online) Momentum dependence of Δ_{xx} and Δ_{xy} determined from the eigenvector corresponding to the leading eigenvalue of the linearized gap equation at $T = 0.006$ eV for Hund's coupling $J = 0.05$ eV (top) and $J = 0.25$ eV (bottom). Gaps of the two xz orbitals are shown in an extended zone scheme. White diamonds indicate the Brillouin-zone boundary. Red (light) and blue (dark) regions correspond to opposite signs of the gap.

$\rightarrow -\Delta_{yx}(p_y, -p_x)$. The latter expression explains the sign change of $\Delta_{xy}(\mathbf{p})$ upon rotation. It is a consequence of the s-wave symmetry in a two-orbital problem where the xz and yz orbitals transform like the two-dimensional coordinates. The fact that the diagonal gap $\Delta_{xx}(\mathbf{p})$ differs for momenta pointing along the two diagonals of the Brillouin zone is a consequence of the fact that the wave functions for the xz and yz orbitals are different (see Ref. 10). Changing the value of the exchange interaction does not change the symmetry of the gap function. However, it significantly affects the momentum dependence of $\Delta_{a_1 a_2}(\mathbf{p})$. As mentioned, the pairing interaction for small J_H is incommensurate with peaks rather far away from the ordering vector $(\pi/a, \pi/a)$ of the antiferromagnetic state in undoped systems at ambient pressure. On the other hand, for $J = 0.25$ eV, the dynamic magnetic susceptibility and the pairing interaction $\Gamma_{pp}(\mathbf{p})$ are peaked very close to $(\pi/a, \pi/a)$. A commensurate pairing interaction can more efficiently change the sign of the gap function in momentum and orbital space, while incommensurations tend to frustrate an optimally shaped pairing gap. This leads to the more complex pairing state for small J.

Finally we determine the consequences of this gap function and analyze the gap anisotropy on the Fermi surface. From the self-energy $\Sigma_{\mathbf{k}}^{\alpha\beta}(i\omega_n)$ we determine the quasiparticle energies $E_{\mathbf{p}}^{*\alpha\beta} = E_{\mathbf{p}}^{\alpha\beta} + \Sigma_{\mathbf{k}}^{\alpha\beta}(0) - \mu\delta_{\alpha\beta}$ and construct the quasiparticle energies of the superconducting state from the eigenvalues of

$$\hat{h}_{\mathbf{p}} = \begin{pmatrix} \hat{E}_{\mathbf{p}}^* & \hat{\Delta}_{\mathbf{p}} \\ \hat{\Delta}_{\mathbf{p}} & -\hat{E}_{-\mathbf{p}}^* \end{pmatrix}. \tag{33}$$

In Fig. 6 we plot the magnitude of the gap along the various sheets of the Fermi surface. The Fermi surface is constructed from the minima of the magnitude of the eigenvalues of $\hat{h}_{\mathbf{p}}$. As shown in Fig. 6(a), we find that in case of a small J the pairing interaction is more incommensurate and the gap vanishes on line nodes on the Fermi surface. However, for larger J values we only find moderately anisotropic gap amplitudes on the Fermi surface [see Figs. 6(b) and 6(c)]. The gap amplitude on the inner Fermi-surface sheet around Γ is significantly larger than the gap on the outer sheet, in agreement with recent ARPES experiments.[16,17] This is a consequence of the fact that $\Delta_{xx}(\mathbf{p})$ and $\Delta_{yy}(\mathbf{p})$ change sign close to the Brillouin-zone center. The gap of the Fermi-surface sheets centered around M is considerably more anisotropic and could be responsible for the observation of anisotropic gaps.[11–14,19] In general, experiments that are sensitive to the minimum of the gap should therefore find much smaller typical gap values and more anisotropic gaps than measurements that are more sensitive to the largest gap values.

Our calculation yields a fully gapped Fermi surface in the case where the pairing interaction is close to being commensurate. In this case the nodes of the gap are located between different Fermi-surface sheets, explaining the dramatic change in the amplitude of the gap as one gets closer to the nodal lines (see Fig. 6). The position of these nodes is not fixed by symmetry and, as is seen in case for more incommensurate pairing interactions, can in principle touch the Fermi surface [see Fig. 6(a)]. It is therefore an interesting
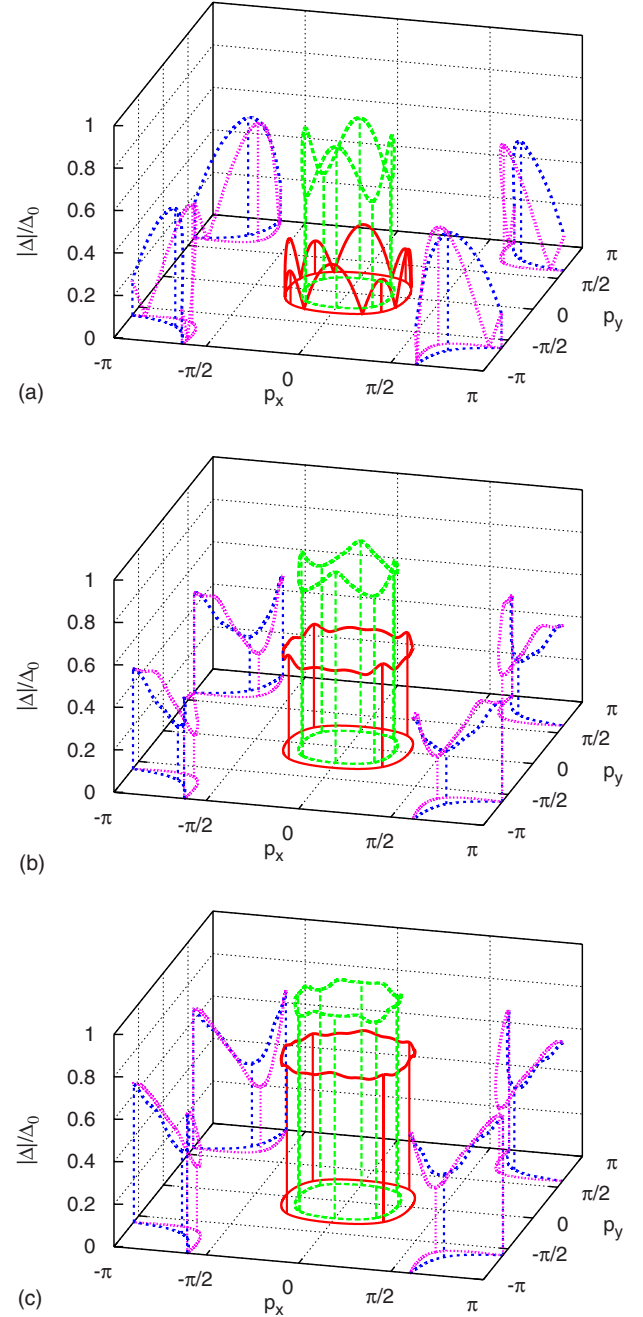

FIG. 6. (Color online) Amplitudes of the gaps along four sheets of the Fermi surface for (a) $J = 0.0$ eV, (b) 0.25 eV, and (c) 0.50 eV. While linearized gap equation cannot define the absolute amplitude Δ_0, the relative gap amplitudes are properly defined.

question to ask what happens if one includes electron-electron overlap between different FeAs layers. This seems particularly relevant for the 122 materials where the outer sheet of the Fermi surface around $\Gamma = (0,0)$ increases its radius for increasing k_z.[32] If the pairing interaction is predominantly two dimensional and determined by those Fermi-surface sheets that are less dispersive in the z direction, we expect that the position of the nodes is only weakly affected by the dispersion along k_z. It is therefore easily possible that at least one Fermi-surface sheet touches the nodal plane for larger k_z values. The intersection between nodal plane and

Fermi surface would then yield a nodal line on the Fermi surface. This implies that one can easily explain fully gapped pairing states and states with line nodes with same pairing symmetry ($s^{\pm}$) and due to the same pairing mechanism. Note that this is impossible for a *d*-wave pairing state, which will always yield line nodes given that the Fermi surface around the Γ point is closed. It is also impossible within a conventional *s*-wave pairing state where the sign of the gap is the same everywhere. Thus, seemingly conflicting observations in different FeAs-based systems do not necessarily imply that there are several distinct pairing mechanisms at work.

In summary, we determined the anisotropy of the spin-fluctuation-induced pairing gap on the Fermi surface of the FeAs-based superconductors. For realistic parameters we find a fully gapped state, while a measurable anisotropy remains for some Fermi-surface sheets. This may explain the conflicting observations for the presence of gap nodes ob-

tained in NMR, penetration depth, and ARPES experiments. It does explain the variation of the gap on distinct sheets of the Fermi surface, as seen in ARPES experiments.[17] More generally, our results demonstrate that a fully gapped superconducting state is fully consistent with an unconventional pairing mechanism.

*Present address: Materials Science and Technology Division, Oak Ridge National Laboratory, Oak Ridge, TN 37831.

[1] Y. Kamihara, T. Watanabe, M. Hirano, and H. Hosono, J. Am. Chem. Soc. **130**, 3296 (2008).

[2] X. H. Chen, T. Wu, G. Wu, R. H. Liu, H. Chen, and D. F. Fang, Nature (London) **453**, 761 (2008).

[3] G. F. Chen, Z. Li, D. Wu, G. Li, W. Z. Hu, J. Dong, P. Zheng, J. L. Luo, and N. L. Wang, Phys. Rev. Lett. **100**, 247002 (2008).

[4] Z.-A. Ren, J. Yang, W. Lu, W. Yi, G.-C. Che, X.-L. Dong, L.-L. Sun, and Z.-X. Zhao, Mater. Res. Innovations **12**, 105 (2008).

[5] H.-H. Wen, G. Mu, L. Fang, H. Yang, and X. Zhu, Europhys. Lett. **82**, 17009 (2008).

[6] L. Boeri, O. V. Dolgov, and A. A. Golubov, Phys. Rev. Lett. **101**, 026403 (2008).

[7] C. de la Cruz, Q. Huang, J. W. Lynn, J. Li, W. Ratcliff II, J. L. Zarestky, H. A. Mook, G. F. Chen, J. L. Luo, N. L. Wang, and P. Dai, Nature (London) **453**, 899 (2008).

[8] I. I. Mazin, D. J. Singh, M. D. Johannes, and M. H. Du, Phys. Rev. Lett. **101**, 057003 (2008).

[9] Z.-J. Yao, J.-X. Li, and Z. D. Wang, arXiv:0804.4166, New J. Phys. (to be published).

[10] X.-L. Qi, S. Raghu, C.-X. Liu, D. J. Scalapino, and S.-C. Zhang, arXiv:0804.4332 (unpublished).

[11] Y. Nakai, K. Ishida, Y. Kamihara, M. Hirano, and H. Hosono, J. Phys. Soc. Jpn. **77**, 073701 (2008).

[12] K. Matano, Z. A. Ren, X. L. Dong, L. L. Sun, Z. X. Zhao, and G. Zheng, Europhys. Lett. **83**, 57001 (2008).

[13] H.-J. Grafe, D. Paar, G. Lang, N. J. Curro, G. Behr, J. Werner, J. Hamann-Borrero, C. Hess, N. Leps, R. Klingeler, and B. Buchner, Phys. Rev. Lett. **101**, 047003 (2008).

[14] H. Mukuda, N. Terasaki, H. Kinouchi, M. Yashima, Y. Kitaoka, S. Suzuki, S. Miyasaka, S. Tajima, K. Miyazawa, P. Shirage, H. Kito, H. Eisaki, and A. Iyo, J. Phys. Soc. Jpn. **77**, 093704 (2008).

[15] T. Kondo, A. F. Santander-Syro, O. Copie, Chang Liu, M. E. Tillman, E. D. Mun, J. Schmalian, S. L. Bud'ko, M. A. Tanatar, P. C. Canfield, and A. Kaminski, Phys. Rev. Lett. **101**, 147003 (2008).

[16] L. Zhao, H. Liu, W. Zhang, J. Meng, X. Jia, G. Liu, X. Dong, G. F. Chen, J. L. Luo, N. L. Wang, L. Wei, G. Wang, Y. Zhou, Y. Zhu, X. Wang, Z. Zhao, Z. Xu, C. Chen, and X. J. Zhou, Chin. Phys. Lett. **25**, 4402 (2008).

[17] H. Ding, P. Richard, K. Nakayama, T. Sugawara, T. Arakane, Y. Sekiba, A. Takayama, S. Souma, T. Sato, T. Takahashi, Z. Wang, X. Dai, Z. Fang, G. F. Chen, J. L. Luo, and N. L. Wang, Europhys. Lett. **83**, 47001 (2008).

[18] R. T. Gordon, N. Ni, C. Martin, M. A. Tanatar, M. D. Vannette, H. Kim, G. Samolyuk, J. Schmalian, S. Nandi, A. Kreyssig, A. I. Goldman, J. Q. Yan, S. L. Bud'ko, P. C. Canfield, and R. Prozorov, arXiv:0810.2295 (unpublished).

[19] C. Martin, R. T. Gordon, M. A. Tanatar, M. D. Vannette, M. E. Tillman, E. D. Mun, P. C. Canfield, V. G. Kogan, G. D. Samolyuk, J. Schmalian, and R. Prozorov, arXiv:0807.0876 (unpublished).

[20] V. Cvetković and Z. Tešanović, arXiv:0804.4678, Europhys. Lett. (to be published).

[21] A. V. Chubukov, D. V. Efremov, and I. Eremin, Phys. Rev. B **78**, 134512 (2008).

[22] A. Chubukov, D. Pines, and J. Schmalian, in *The Physics of Conventional and Unconventional Superconductors*, edited by K. H. Bennemann and J. B. Ketterson (Springer-Verlag, Berlin, 2002).

[23] W. Z. Hu, J. Dong, G. Li, Z. Li, P. Zheng, G. F. Chen, J. L. Luo, and N. L. Wang, Phys. Rev. Lett. **101**, 257005 (2008).

[24] S. E. Sebastian, J. Gillett, N. Harrison, P. H. C. Lau, C. H. Mielke, and G. G. Lonzarich, J. Phys.: Condens. Matter **20**, 422203 (2008).

[25] X. F. Wang, T. Wu, G. Wu, H. Chen, Y. Xie, J. Ying, Y. Yan, R. Liu, and X. Chen, arXiv:0806.2452 (unpublished).

[26] T. Kroll, S. Bonhommeau, T. Kachel, H. A. Duerr, J. Werner, G. Behr, A. Koitzsch, R. Huebel, S. Leger, R. Schoenfelder, A. Ariffin, R. Manzke, F. M. F. de Groot, J. Fink, H. Eschrig, B. Buechner, and M. Knupfer, Phys. Rev. B **78**, 220502 (2008).

[27] Q. Si and E. Abrahams, Phys. Rev. Lett. **101**, 076401 (2008).

[28] M. Daghofer, A. Moreo, J. A. Riera, E. Arrigoni, D. J. Scalapino, and E. Dagotto, Phys. Rev. Lett. **101**, 237004 (2008).

[29] N. F. Berk and J. R. Schrieffer, Phys. Rev. Lett. **17**, 433 (1966).

[30] K. Kuroki, S. Onari, R. Arita, H. Usui, Y. Tanaka, H. Kontani, and H. Aoki, Phys. Rev. Lett. **101**, 087004 (2008).

[31] D. J. Singh and M.-H. Du, Phys. Rev. Lett. **100**, 237003 (2008).

[32] C. Liu, T. Kondo, M. E. Tillman, R. Gordon, G. D. Samolyuk, Y. Lee, C. Martin, J. L. McChesney, S. Bud'ko, M. A. Tanatar, E. Rotenberg, P. C. Canfield, R. Prozorov, B. N. Harmon, and A. Kaminski, arXiv:0806.2147 (unpublished).

[33] S. Raghu, X.-L. Qi, C.-X. Liu, D. J. Scalapino, and S.-C. Zhang, Phys. Rev. B **77**, 220503(R) (2008).

[34] T. Takimoto, T. Hotta, and K. Ueda, Phys. Rev. B **69**, 104504 (2004).

[35] J. Schmalian, Phys. Rev. Lett. **81**, 4232 (1998); J. Schmalian, M. Langer, S. Grabowski, and K. H. Bennemann, Phys. Rev. B **54**, 4336 (1996).

[36] N. E. Bickers, D. J. Scalapino, and S. R. White, Phys. Rev. Lett. **62**, 961 (1989).

[37] A. V. Chubukov and J. Schmalian, Phys. Rev. B **72**, 174520 (2005).